Pergamon

Geochimica et Cosmochimica Acta, Vol. 59, No. 14, pp. 2869–2882, 1995

0016-7037/95 $9.50 + .00

0016-7037(95)00182-4

Equation of state for the NaCl–H_2O–CO_2 system: Prediction of phase equilibria and volumetric properties

ZHENHAO DUAN, NANCY MØLLER, and JOHN H. WEARE
Department of Chemistry, University of California, San Diego, La Jolla, CA 92093-0340, USA

(*Received August* 9, 1994; *accepted in revised form April* 17, 1995)

Abstract—An equation of state (EOS) has been developed for the NaCl–H_2O–CO_2 system which consistently predicts various properties including *PVTX*, immiscibility or phase equilibria, solubilities, and activities with an accuracy close to that of experimental data from 300 to about 1000°C and 0–6000 bar with NaCl concentrations to about 30 wt% of NaCl (relative to NaCl + H_2O) or to about 50 wt% with less accuracy. The EOS predicts that excess volumes can be over 30% of the total volume under some *T-P* conditions. Adding NaCl to the H_2O–CO_2 system dramatically increases the *T-P* range of immiscibility. The immiscibility field is minimal around 400–500°C. Above or below this temperature, it expands for a constant pressure. A moderately saline brine can evolve into a very saline brine by phase separation at high temperatures. The presence of NaCl can substantially decrease the activity of H_2O and increase that of CO_2, thus affecting decarbonation and dehydration reactions. Compared to the EOS of Bowers and Helgeson (1983a), the EOS of this study is more reliable in the calculation of volumetric properties particularly in the low pressure range. In addition, BH EOS cannot predict phase equilibria.

1. INTRODUCTION

H_2O, CO_2, and NaCl are the most frequently encountered species in natural fluids. The knowledge of pressure-volume-temperature (*PVT*) properties, phase equilibria (or immiscibilities), and chemical potentials (or activities) is essential to the understanding of mechanisms of various geological processes. For example, the properties of systems as diverse as oil deposits (Alston et al., 1985), Mississippi-valley ore deposits (Hanor, 1979), porphyry ore deposits (Ramboz, 1979), circulating seafloor hydrothermal fluids (Welhan and Craig, 1979; Bischoff, 1980), geothermal fluids (Truesdell, 1993), and metamorphic fluids (Crawford, 1981) may be controlled by fluid immiscibility. The presence of NaCl in fluids can substantially change their thermodynamic properties. For example, the addition of NaCl into the CO_2–H_2O system can greatly increase the *T-P* range of immiscibility. Above the critical temperature of H_2O (374°C), there is no immiscibility for the binary H_2O–CO_2. However, the immiscible field may exist well above this temperature if NaCl is added. Immiscibility has a profound impact on the transportation of many ore-forming elements (W. Hu et al., unpubl. data) in hydrothermal processes and geothermal venting. Understanding the properties of the NaCl–H_2O–CO_2 system is also essential to the prediction of mixed volatile equilibria in metamorphic settings and to the interpretation of observations made on fluid inclusions. In addition, *PVT* properties have been extensively used in the interpretation of fluid inclusion data (Ramboz et al., 1985; Diamond, 1990).

Prior to this work, the only equation of state (EOS) available for the NaCl–H_2O–CO_2 system was that of Bowers and Helgeson (1983a). As reviewed by Brown and Lamb (1989), that EOS reproduces the data of Gehrig (1980) at moderate densities, but extrapolates poorly to higher density mixtures. Furthermore, it cannot predict phase behavior, which is a major limitation for geochemical applications. In order to calculate isochores of this system for fluid inclusion studies, Brown and Lamb (1989) proposed "ideal geometrical" mixing of H_2O–NaCl and CO_2. They linearly interpolate isochores between the endmember CO_2 and the binary H_2O–NaCl. This provides an approximate means for isochore calculations. However, there are large errors because the excess volume of mixing H_2O–NaCl and CO_2 can be 10–30% of the total volume of the mixture. In addition, it is not possible to obtain other thermodynamic information (such as chemical potentials or phase behavior) from this method.

The purpose of this study is to develop an EOS which can predict both volumetric properties and phase equilibria for the system NaCl–H_2O–CO_2 up to high temperatures and high pressures. Recently Anderko and Pitzer (1993) successfully developed an EOS for the NaCl–H_2O system based on the methods introduced by Dimitrelis and Prausnitz (1986). This equation can predict both *PVT* properties and phase equilibria in this binary to high temperatures (>300°C). A comprehensive study of various EOS reveals that this approach gives the most accurate representation of salt-containing systems. In this study, the same approach is adopted for the NaCl–H_2O–CO_2 system. The resulting EOS consistently predicts various properties including phase equilibria (or immiscibilities), activities, and volumetric properties with an accuracy close to that of experiments. Since the EOS of this study treats NaCl as ion-pair molecule, it is not reliable for temperature below 300°C, where the dissociation of NaCl is substantial. We note that this work does not replace our earlier EOS (Duan et al., 1992a,b) for salt-free systems which is more accurate for temperatures below 350°C.

2. THE EQUATION OF STATE

The form of an EOS is generally chosen on the basis of its ability to describe a system with accuracy over a range of the data used in the parameter adjustment. To improve extrapolation beyond the range of data, forms justified by approximate theoretical results (e.g., the virial equation, hard-sphere gas results, etc.) are usually selected. However, these forms can only yield qualitative results. In all cases,

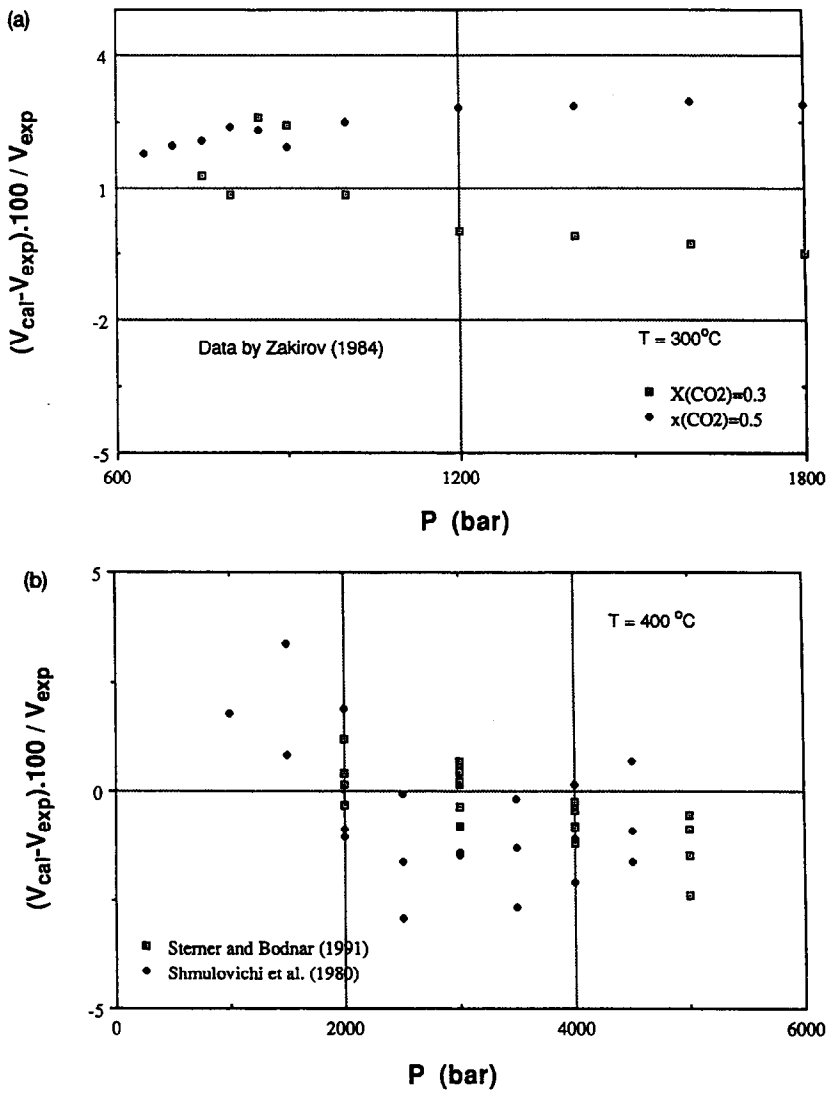

FIG. 1. Comparisons of experimental molar volumes in the binary CO_2–H_2O as a function of pressure with the predictions of the EOS of this study (a) T = 300°C; (b) T = 400°C; (c) T = 500°C; (d) T = 700°C.

accurate representations must contain parameters which are evaluated from experimental data. The parameters for endmembers are usually evaluated from pure system data. Then a mixing rule, which properly combines the endmember parameters, is developed to accurately reproduce mixture data. There are a number of different kinds of EOS, each having strengths and weaknesses. For example, cubic EOS such as the Peng-Robinson's equation (Skryjek and Vera, 1986) predicts phase equilibria well for nonaqueous systems, but provides poor pre-

Table 1. The Parameters for CO_2

μ_{CO_2}	0
b_{CO_2}	49.52
a_{CO_2}	$(3.86491553-2.36222839/Tr+3.51977858/Tr^2-1.01456034/Tr^4).10^6$
$(ac)_{CO_2}$	-4.18508460e+06+5.18786559e+05/Tr
$(ad)_{CO_2}$	1.49548462e+07+1.40232739e+06/Tr
$(ae)_{CO_2}$	-3.04732284e+07

Tr = T/304.2

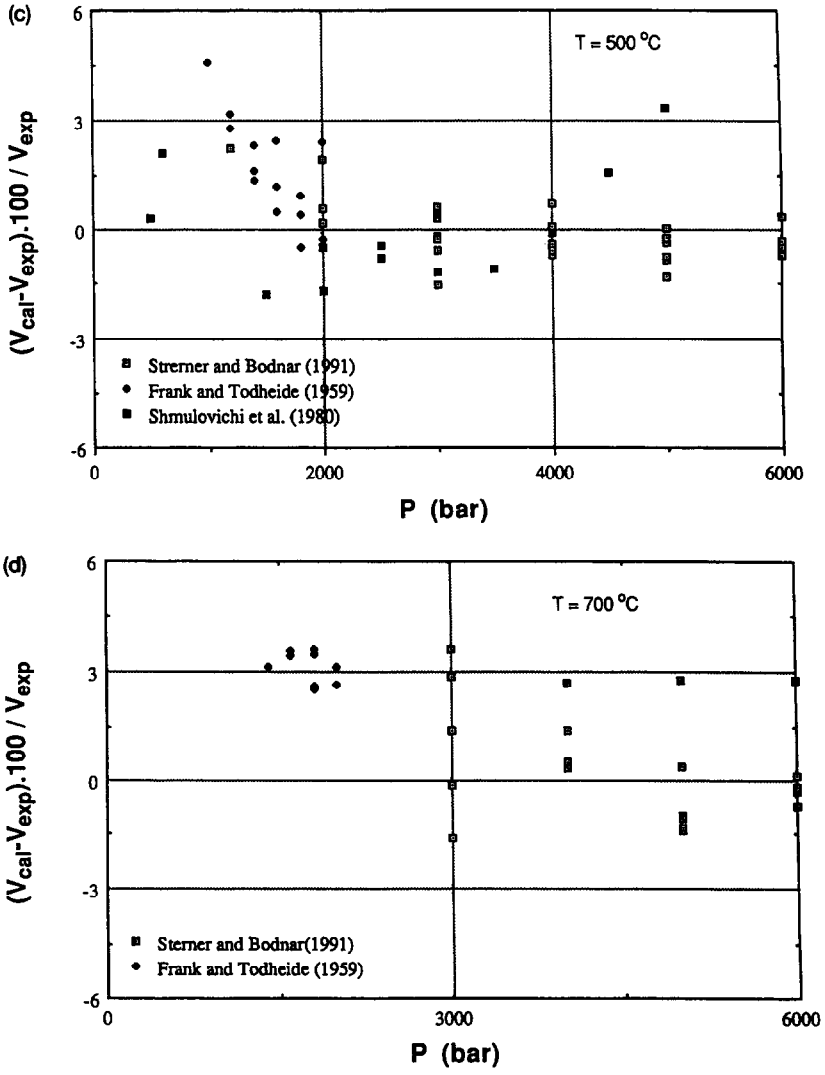

FIG. 1. (Continued)

dictions of volumetric properties. The EOS developed by Duan et al. (1992b) is accurate in the $CH_4-CO_2-H_2O$ system over a large *T-P* range, but has difficulties in salt-bearing systems like the $NaCl-H_2O-CO_2$ system.

In the approach of Anderko and Pitzer (1993) and Dimitrelis and Prausnitz (1986), the system is first idealized as composed of species with complex but treatable interactions such as a system of hard spheres and dipoles. The idealized system, called the reference system, is described quantitatively using some theory with well-defined assumptions. Corrections are then added to account for differences between the real and the idealized systems. The corrections, called perturbations, are empirical. For Helmholtz free energy this gives

$$a = a^{ref} + a^{per}. \quad (1)$$

For correlation and prediction of phase behavior of nonpolar systems, Dimitrelis and Prausnitz (1986) used a hard-sphere mixture as a reference system. Because NaCl and H_2O are strong polar molecules at high temperatures, Anderko and Pitzer (1993) added a term representing the dipolar hard sphere contribution (i.e., the difference of Helmholtz energy of dipolar hard spheres and that of simple hard spheres). We found that the use of the dipolar hard sphere term is essential to capture the behavior of the complex salt containing system. This leads to

$$a = a^{hd} + a^{dip} + a^{per}. \quad (2)$$

The compressibility factor Z can be derived from the Helmholtz energy using the relation,

$$Z = -v[\partial(a/RT)/\partial v]_T. \quad (3)$$

Table 2. The Interaction Parameters for the Binary H_2O-CO_2

α_{ij}	0.88868-1.7347e-04 T+4.038e-07 T^2
γ_{iij}, γ_{ijj}	1.41683554-7.02857143D-04 T if T<773 K 1.03463-0.0002 T if T≥773 K
δ_{iiij}, δ_{iijj}, δ_{ijjj}	1.0
ε_{iiij}, ε_{iijj}, ε_{ijjj}, ε_{jjjj}	1.28262-7.32919762e-04 T+3.51190476e-07 T^2

i and j represent CO_2 and H_2O.

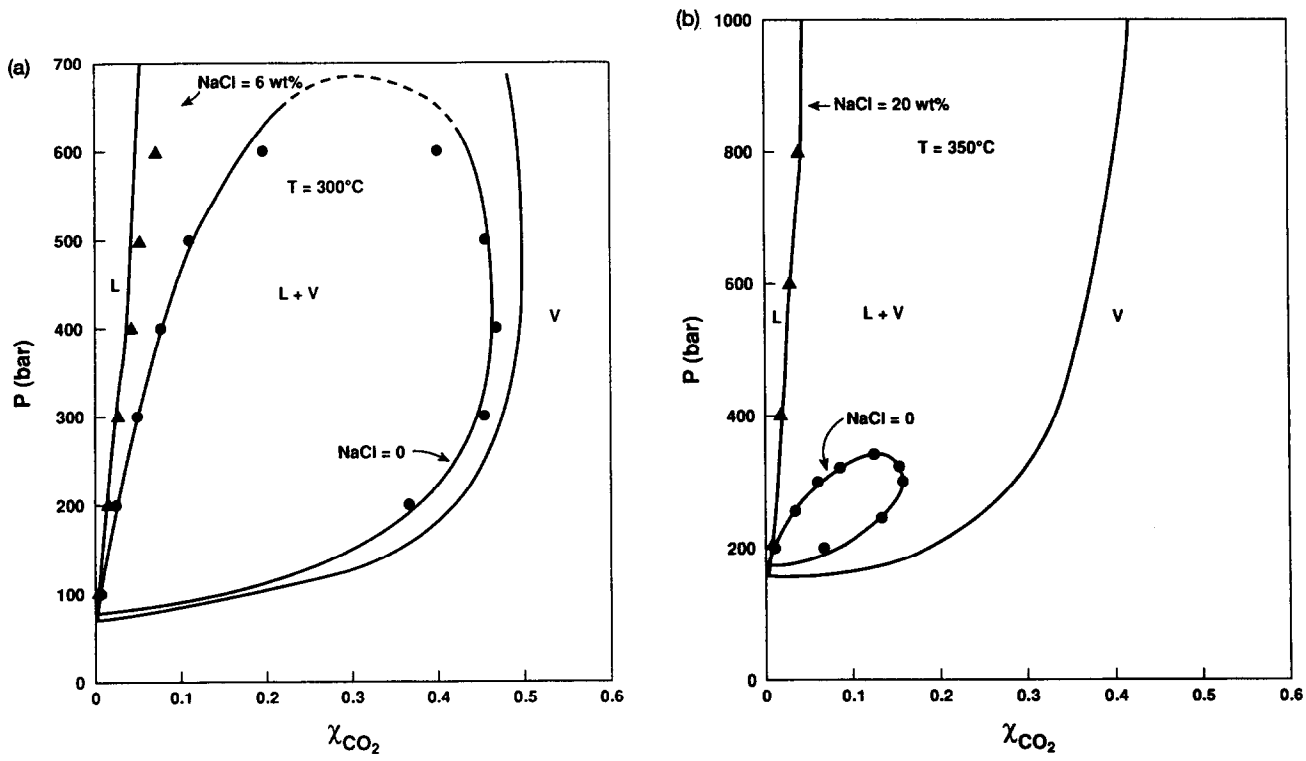

FIG. 2. (a) Vapor-liquid coexistence in the CO_2–H_2O and in the NaCl–H_2O–CO_2 systems at 300°C. The solid lines: EOS of this study; the symbols: experimental data by Todheide and Franck (1963) and Takenouchi and Kennedy (1965). (b) Vapor-liquid coexistence in the CO_2–H_2O and in the NaCl–H_2O–CO_2 systems at 350°C. The solid lines and the symbols are the same as in (a).

It follows that

$$Z = \frac{PV}{RT} = Z^{hd} + Z^{dip} + Z^{per}. \quad (4)$$

$$Z_{hd} = \frac{1 + \left(\frac{3DE}{F} - 2\right)\eta + \left(\frac{3E^3}{F^2} - \frac{3DE}{F} + 1\right)\eta^2 - \frac{E^3}{F^2}\eta^3}{(1-\eta)^3}, \quad (5)$$

where

$$D = \sum_{i=1}^{n} x_i\sigma_i, \quad (6)$$

$$E = \sum_{i=1}^{n} x_i\sigma_i^2, \quad (7)$$

$$F = \sum_{i=1}^{n} x_i\sigma_i^3, \quad (8)$$

2.1. The Hard Sphere Contribution

By comparison with experimental phase equilibria data from nonpolar systems, Dimitrelis and Prausnitz (1986) found that the equation for hard spheres developed by Boublik (1970) and Mansoori et al. (1971) is superior to that by Carnahan and Starling (1969). Therefore, this expression, which is good for both pure systems and mixtures of different radius hard spheres, is adopted for the hard-sphere reference term.

Table 3. The Interaction Parameters for the Binary NaCl–CO_2

α_{ij}	-1.73355444+5.60408826e-03 T-2.70381422e-06 T^2
γ_{iij}, γ_{ijj}	1.41683554-7.02857143e-04 T if T<773 K 1.03463 - 0.0002 T if T≥773 K
δ_{iiij}, δ_{iijj}, δ_{ijjj}	1.0
ε_{iiij}, ε_{iijj}, ε_{ijjj}, ε_{jjjj}	1.28262-7.32919762e-04 T+3.51190476e-07 T^2

i and j represent NaCl and CO_2.

Table 4. Comparison of the Data of Gehrig (1980) with Those of Bischoff (1991)

T(°C)	P (bar)	x_{NaCl}	x_{H_2O}	v(Bischoff)	v(Gehrig)
500	556	0.0193	0.9807	51.43	48.34
430	363	0.0193	0.9807	37.62	40.94

$$\eta = \frac{\left(\sum_i^n \sum_j^n x_i x_j [(b_i^{1/3} + b_j^{1/3})/2]^3\right)}{4v} = \frac{\pi N_A F}{6v}. \quad (9)$$

In this expression, v is molar volume, b is the van der Waals covolume, and N_A is Avogadro's number. As can be seen, only one parameter b_i for each species needs to be determined (by placing $x_i = 1$ in Eqns. 8 and 9), because σ_i can be found from Eqns. 8 and 9. The value of b_i is determined by fitting experimental data of endmember systems.

2.2. The Dipolar Contribution

The expression for the dipolar hard-sphere Helmholtz energy developed by Stell et al. (1972, 1974) and Rushbrooke et al. (1973) and the mixing rule by Twu et al. (1975) and Gubbins and Twu (1978) are adopted for the dipolar contribution in the mixture system.

$$Z_{dip} = \eta \frac{\left(1 - \frac{2A_3}{A_2}\right)\frac{\partial A_2}{\partial \eta} + \frac{\partial A_3}{\partial \eta}}{\left(1 - \frac{A_3}{A_2}\right)^2}, \quad (10)$$

where

$$A_2 = -\frac{4}{3}\sum_{i=1}^n \sum_{j=1}^n x_i x_j \frac{b_i b_j}{b_{ij}^2} \eta_{ij} \tilde{\mu}_i^2 \tilde{\mu}_j^2 I_2(\eta), \quad (11)$$

$$A_3 = \frac{10}{9}\sum_{i=1}^n \sum_{j=1}^n \sum_{k=1}^n x_i x_j x_k \frac{b_i b_j b_k}{b_{ij} b_{ik} b_{jk}} \eta_{ijk}^2 \tilde{\mu}_i^2 \tilde{\mu}_j^2 \tilde{\mu}_k^2 I_3(\eta), \quad (12)$$

$$\frac{\partial A_2}{\partial \eta} = -\frac{4}{3}\sum_{i=1}^n \sum_{j=1}^n x_i x_j \frac{b_i b_j}{b_{ij} b} \tilde{\mu}_i^2 \tilde{\mu}_j^2 \left(I_2(\eta) + \eta \frac{\partial I_2(\eta)}{\partial \eta}\right) \quad (13)$$

$$\frac{\partial A_3}{\partial \eta} = \frac{10}{9}\sum_{i=1}^n \sum_{j=1}^n \sum_{k=1}^n x_i x_j x_k \frac{b_i b_j b_k}{b_{ij} b_{jk} b_{ik}} \frac{(b_{ij} b_{jk} b_{ik})^{2/3}}{b^2} \times \tilde{\mu}_i^2 \tilde{\mu}_j^2 \tilde{\mu}_k^2 \left(2I_3(\eta) + \eta \frac{\partial I_3(\eta)}{\partial \eta}\right)\eta, \quad (14)$$

where

$$\eta_{ij} = b_{ij}/4v, \quad (15)$$

$$\eta_{ijk} = b_{ijk}/4v = (b_{ij} b_{ik} b_{jk})^{1/3}/4v, \quad (16)$$

$$b_{ij} = [(b_i^{1/3} + b_j^{1/3})/2]^3, \quad (17)$$

$$I_2(\eta) = 1 + c_1\eta + c_2\eta^2 + c_3\eta^3, \quad (18)$$

$$\frac{I_3(\eta)}{I_2(\eta)} = 1 + c_4\eta + c_5\eta^2 + c_6\eta^3, \quad (19)$$

$$\frac{\partial I_2}{\partial \eta} = c_1 + 2c_2\eta + 3c_3\eta^2, \quad (20)$$

$$\frac{\partial I_3}{\partial \eta} = (c_1 + 2c_2\eta + 3c_3\eta^2)(1 + c_4\eta + c_5\eta^2 + c_6\eta^3) + (1 + c_1\eta + c_2\eta^2 + c_3\eta^3)(c_4 + 2c_5\eta + 3c_6\eta^2). \quad (21)$$

b_i is the endmember van der Waals covolume and is evaluated from experimental data. Fitting c_i, the parameters of the $I_2(\eta)$ and $I_3(\eta)$ functions, to the results from the hard-sphere equations of Rushbrooke et al. (1973) yields: $c_1 = 1.6054$, $c_2 = -4.4521$, $c_3 = 10.0368$, $c_4 = 0.35147$, $c_5 = -1.83943$, and $c_6 = 5.95676$. η and $\tilde{\mu}_i$ in the above expressions are obtained by

$$\eta = \frac{b}{4v} = \frac{1}{4v}\sum_{i=1}^n \sum_{j=1}^n x_i x_j b_{ij}, \quad (22)$$

$$\tilde{\mu}_i = \left(\frac{\theta^2}{\sigma^3 kT}\right)^{1/2}, \quad (23)$$

where θ is dipole moment, k is Boltzmann constant, and b can be calculated in Eqn. 22. Therefore, μ is the only parameter to be determined by fitting to dipole moment measurements.

2.3. The Perturbation Contribution

The perturbation contribution accounts for effects which cannot be represented by the hard-sphere term and the dipole hard-sphere term. Anderko and Pitzer (1993) developed the following expression for the perturbation contribution of mixtures:

$$Z_{per} = -\frac{1}{RT}\left(\frac{a}{v} + \frac{acb}{2v^2} + \frac{3adb^2}{16v^3} + \frac{aeb^3}{16v^4}\right). \quad (24)$$

In this equation, the quantities a, acb, adb^2, and aeb^3 are related to the second, third, fourth, and fifth virial coefficients. These parameters together with b are evaluated from endmember (pure system) experimental data and the following mixing rules:

$$a = \sum_{i=1}^n \sum_{j=1}^n x_i x_j a_{ij}, \quad (25)$$

$$acb = \sum_{i=1}^n \sum_{j=1}^n \sum_{k=1}^n x_i x_j x_k (ac)_{ijk} b_{ijk}, \quad (26)$$

Table 5. Ternary Interaction Parameters for the NaCl–H_2O–CO_2 System

Υ_{ijk}	-0.207+0.00227 T-1.051e-06 T^2
δ_{iijk} , δ_{ijjk} , δ_{ijkk}	1.0
ε_{iiijk} , ε_{iijjk} , ε_{ijjkk} , ε_{ijjjk} , b_{ijjkk} , b_{ijkkk}	1.28262-7.32919762e-04 T+3.51190476e-07 T^2

i, j and k represent NaCl, H_2O and CO_2.

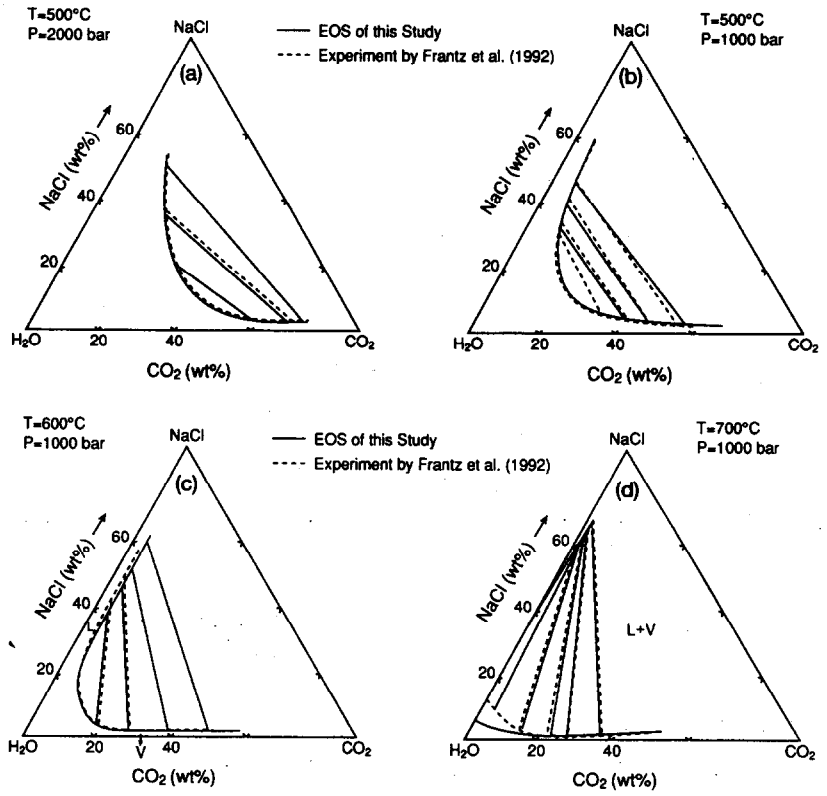

FIG. 3. Comparison of experimental phase equilibria (measured by synthetic fluid inclusion method) in the ternary $NaCl-H_2O-CO_2$ with the prediction of the EOS of this study. (a) 500°C, 2000 bar; (b) 500°C, 1000 bar; (c) 600°C, 1000 bar; (d) 700°C, 1000 bar).

$$adb^2 = \sum_{i=1}^{n}\sum_{j=1}^{n}\sum_{k=1}^{n}\sum_{l=1}^{n} x_i x_j x_k x_l (ad)_{ijkl} b^2_{ijkl}\,, \tag{27}$$

$$aeb^3 = \sum_{i=1}^{n}\sum_{j=1}^{n}\sum_{k=1}^{n}\sum_{l=1}^{n}\sum_{m=1}^{n} x_i x_j x_k x_l x_m (ae)_{ijklm} b^3_{ijklm}\,, \tag{28}$$

The mixing parameters in Eqns. 25–28 are related to the endmember parameters by the following equations:

$$b_{ijk} = [(b_i^{1/3} + b_j^{1/3} + b_k^{1/3})/3]^3, \tag{29}$$

$$b_{ijkl} = [(b_i^{1/3} + b_j^{1/3} + b_k^{1/3} + b_l^{1/3})/4]^3, \tag{30}$$

$$b_{ijklm} = [(b_i^{1/3} + b_j^{1/3} + b_k^{1/3} + b_l^{1/3} + b_m^{1/3})/5]^3, \tag{31}$$

$$a_{ij} = (a_i a_j)^{1/2}\alpha_{ij}\,, \tag{32}$$

$$(ac)_{ijk} = [(ac)_i (ac)_j (ac)_k]^{1/3}\gamma_{ijk}\,, \tag{33}$$

$$(ad)_{ijkl} = [(ad)_i (ad)_j (ad)_k (ad)_l]^{1/4}\delta_{ijkl}\,, \tag{34}$$

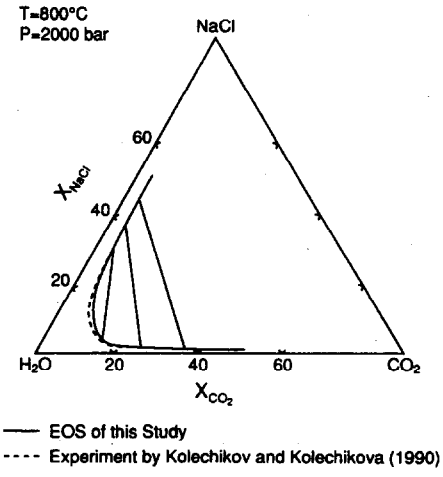

FIG. 4. The prediction of immiscibility boundary in the ternary $NaCl-H_2O-CO_2$ at 800°C and 2000 bar.

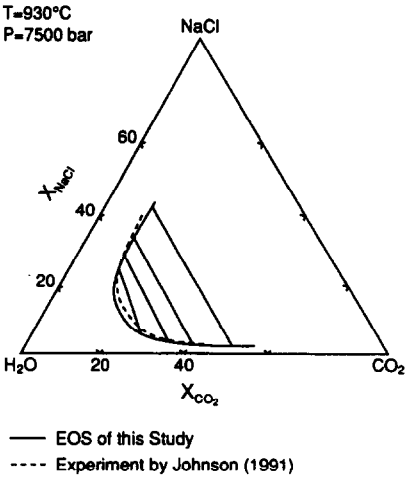

FIG. 5. The prediction of immiscibility boundary (measured by synthetic fluid inclusion method) in the ternary $NaCl-H_2O-CO_2$ at 930°C and 7500 bar.

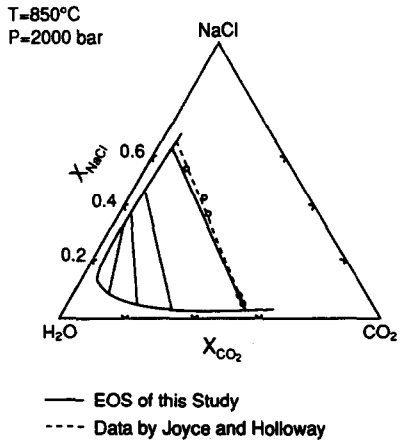

FIG. 6. Comparison of experimental immiscibility boundary (measured using hydrogen and oxygen buffer) in the ternary NaCl–H_2O–CO_2 at 850°C and 2000 bar with the prediction of the EOS of this study.

$$(ae)_{ijklm} = [(ae)_i(ae)_j(ae)_k(ae)_l(ae)_m]^{1/5}\epsilon_{ijklm}, \quad (35)$$

where α_{ij}, γ_{ijk}, δ_{ijkl}, and ϵ_{ijklm} are interaction parameters which are evaluated from mixed system data.

3. EVALUATION OF EXPERIMENTAL DATA AND PARAMETERIZATION

The system NaCl–H_2O–CO_2 includes three pure systems (NaCl, H_2O, and CO_2), three binaries (NaCl–H_2O, NaCl–CO_2, and H_2O–CO_2), and one ternary. The parameters for pure NaCl and H_2O and the binary interaction parameters for NaCl–H_2O mixtures are taken from Anderko and Pitzer (1993). The thermodynamic properties for pure CO_2 and CO_2–H_2O are well predicted by the EOS of Duan et al. (1992a,b). However, the form of that EOS is different from that of the EOS presented here. Therefore, we need to evaluate the parameters for pure CO_2, the binary mixture interaction parameters for CO_2–H_2O and NaCl–CO_2, and the ternary interaction parameters for NaCl–H_2O–CO_2. Because there is little experimental data on systems with NaCl concentrations larger than 25 wt% (relative to NaCl + H_2O), where liquid + solid NaCl field lies, the EOS of this study does not include the prediction of halite solubility and may be less accurate for high NaCl concentration systems.

3.1. CO_2

CO_2 has no permanent dipole moment, so $\mu_{CO_2} = 0$ and $Z_{dip} = 0$. The van der Waals covolume of CO_2, b_{CO_2}, and a, ac, ad, ae in Eqn. 24 are found from the *PVT* data of CO_2. These data were reviewed by Duan et al. (1992a). 1846 data points, covering a range of 300–1000°C and 0–8000 bar were used in the evaluation on these parameters. All the datasets agree with each other within about 0.1–0.5% for pressures below 3500 bar. Above 3500 bar the deviation between datasets can be as much as 2.5%. The parameters for this EOS are listed in Table 1. The fit to the data has an average error in volume of 1.2%. The maximum deviation of the fit is 4.1% at 3500 bar and 320°C.

3.2. CO_2–H_2O

Many *PVT* and phase equilibria data for this binary system have been reported. These data have been reviewed by Duan et al. (1992b). It was found that most of the *PVTX* data agree within about 5%. There was some deviations in the phase equilibrium data. The reported compositions of the coexisting vapor phase differ by as much as 16% between Takenouchi and Kennedy (1964) and Todheide and Franck (1963). Recently, Sterner and Bodnar (1991) and Mather and Franck (1992) remeasured the equilibrium composition and found agreement of Todheide and Frank's data.

All the *PVTX* data above 300°C listed in Table 3 of Duan et al. (1992b), plus the phase data by Todheide and Franck (1963) and Mather and Franck (1992) are used in the evaluation of H_2O–CO_2 binary interaction parameters (Table 2). With this parameterization, it is shown by Fig. 1 that the EOS of this study can predict volumes in this binary with maximum deviation of about 5%. This is about the same accuracy as the EOS of Duan et al. (1992b). Figure 2a,b shows that the EOS described here can also predict phase equilibria accurately except for the critical region. D. B. Joyce and J. G. Belencoe (pers. commun.) measured the activities of H_2O in this binary from 400 to 700°C at 500 bar using a hydrogen and oxygen fugacity buffer. These measurements can be predicted by the EOS of this study within the error bars except at 400°C. This is similar to the performance of our earlier EOS (Duan et al., 1992b) for temperatures above 350°C.

3.3. NaCl–CO_2

Solubilities of CO_2 in molten NaCl have been studied by Gjothiem et al. (1962) in the temperature range 850–950°C at a CO_2 pressure of 1 atm. At 850 and 950°C, the solubilities of CO_2 in NaCl are 4.6×10^{-6} and 6.0×10^{-6} moles of CO_2 per cm^3 of solvent, respectively. It is very likely that the NaCl solubility in the CO_2 vapor phase is smaller. Thus, CO_2 and NaCl are almost immiscible in the *T-P* range of the present study. However, the concentrations of both NaCl and CO_2 in

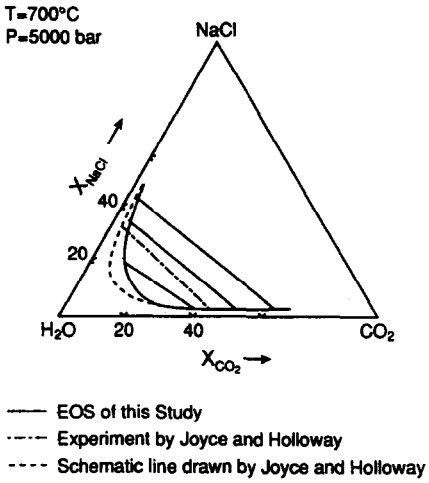

FIG. 7. Calculation of phase equilibria at 700°C and 5000 bar and comparison with experimental data (measured using hydrogen and oxygen buffer). The dashed line is a schematic immiscibility boundary drawn by Joyce and Holloway (1993).

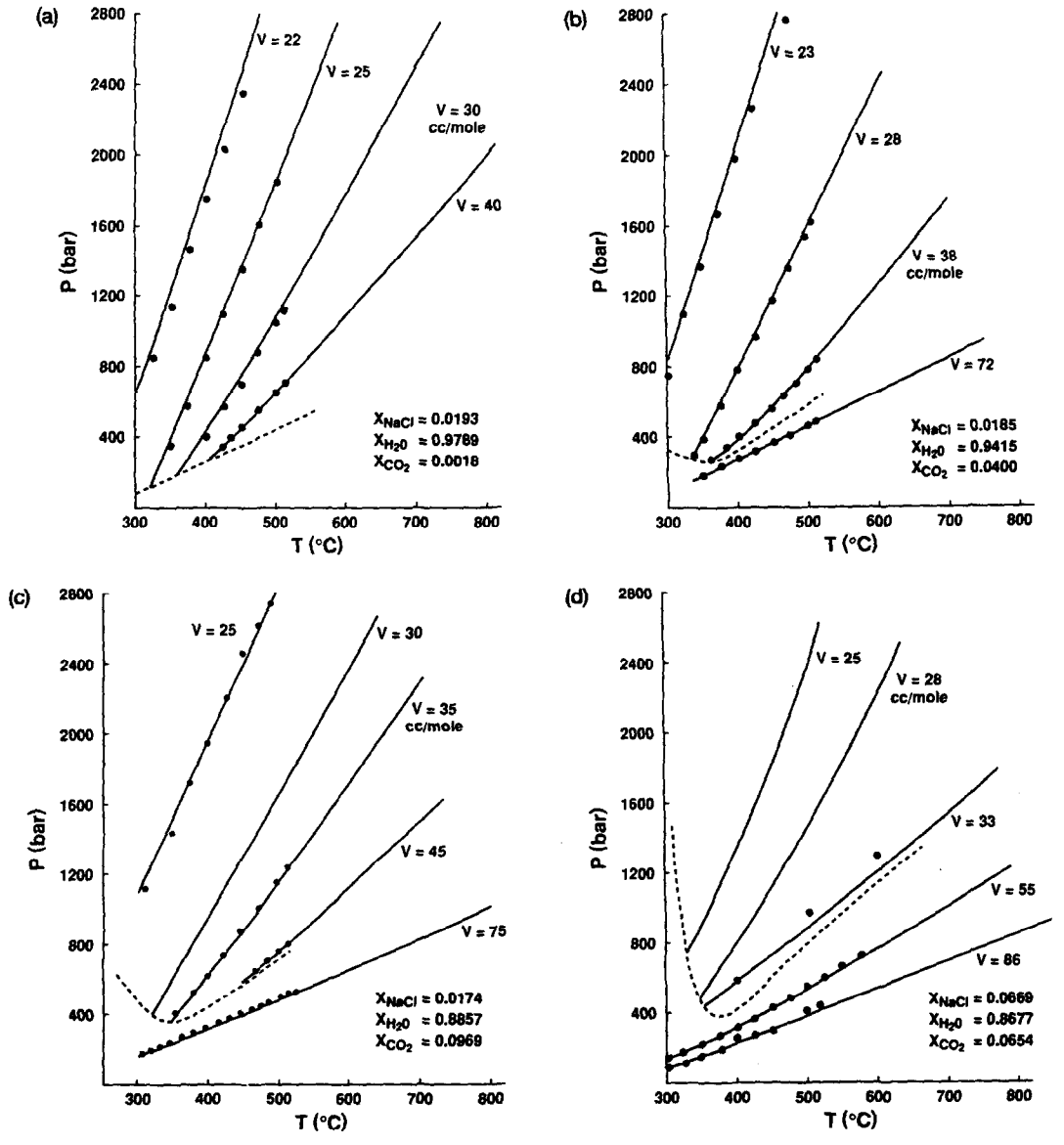

FIG. 8. (a)–(d) Comparison of experimental *PVTX* properties in the ternary NaCl–H_2O–CO_2 with prediction of the EOS of this study. Symbols: the experimental data of Gehrig (1980); The dashed line: the predicted phase boundary. Below this boundary is the liquid-vapor two phase field and above the boundary is the single fluid phase field, solid lines: isochores. CP stands for critical point.

H_2O-containing fluids can be very high and the interaction between them is not negligible. It follows that we have to evaluate the CO_2–NaCl interaction parameters directly from the ternary data as discussed below. The parameters are listed in Table 3. Because there are few experiments on systems with NaCl concentrations larger than 25 wt%, we cannot assess the validity of our new EOS for highly saline ternary compositions.

3.4. NaCl–H_2O–CO_2

The most extensive *PVTX* dataset for this ternary system, about 5000 experimental data points covering temperature range from about 200–560°C and pressure range from 0 to 3000 bar, has been reported by Gehrig (1980). Note that his original data need 0.4–2.9% correction (depending on temperature) in volume because of thermal expansion of aparatus. Since this is the only comprehensive *PVTX* dataset in this *T-P* range, we can only roughly estimate its uncertainty. The binary H_2O–NaCl density data reported by Gehrig (1980) agree with densities interpolated from data reported by Bodnar (1985) within about 4% for pressures above 1000 bar. For pressures below 1000 bar, the deviation of the Gehrig (1980) data from those of Bischoff (1980) is about 7% as indicated by Table 4. In addition to these data, Johnson (1992) measured isochore locations using synthetic fluid inclusions with x_{CO_2} ranging from 0.1–0.51 and relative salinities of 6–23.9 wt% around 7000 bar and 900°C.

Besides the *PVTX* data, Takenouchi and Kennedy (1965) reported CO_2 solubility data in NaCl aqueous solution from

Table 6. Comparison of experimental mole volumes with EOS

T(K)	P(bar)	x_{NaCl}	x_{H_2O}	x_{CO2}	v(BH)	V(DMW)	v(exp)	err(BH)	err(DMW)
733	416	.0193	.9789	.0018	40.53	57.94	61.14	-33.71	-5.23
733	435	.0191	.9688	.0121	42.45	56.19	57.88	-26.66	-2.92
713	406	.0186	.9439	.0375	45.74	58.62	62.03	-26.26	-5.49
713	403	.0185	.9415	.0400	47.83	60.48	61.14	-21.77	-1.08
703	407	.0183	.9303	.0514	44.89	55.31	58.08	-22.72	-4.77
733	517	.0183	.9303	.0514	45.88	49.45	51.97	-11.71	-4.85
703	412	.0180	.9146	.0674	51.35	59.46	61.14	-16.02	-2.75
733	402	.0324	.9463	.0213	48.22	66.20	66.24	-27.20	-.05
743	457	.0324	.9463	.0213	44.31	56.30	56.05	-20.94	.45
713	400	.0317	.9252	.0431	44.97	58.56	57.06	-21.19	2.62
763	403	.0714	.9259	.0027	39.22	70.96	71.33	-45.01	-.52
713	423	.0669	.8677	.0654	42.86	53.00	56.05	-23.53	-5.43

The volume are in cm^3/mole. v(BH) , v(DMW) are the mole volumes calulated by the EOS of Bowers and Helgeson (1983a) and by the EOS of this study, respectively. v(exp) is experimental mole volume By Gehrig (1980). $err=(v_{EOS} - v_{exp}).100/v_{exp}$.

300 to 400°C. Recently, Kotelnikov and Kotelnikova (1990) and Frantz et al. (1992) measured immiscibilities using synthetic fluid inclusions. The data of Frantz et al. (1992) range from 500 to 700°C and 1000–3000 bar. Except for the diagram at 600°C and 3000 bar, all the others have sufficient data to delineate the immiscibility boundaries and tie lines. The data of Kotelnikov and Kotelnikova (1990) covers a temperature range from 400 to 800°C and pressure range from 1000 bar to 2000 bar. We were unable to delineate the phase boundaries from this dataset except in the cases of 600 and 800°C at 2000 bar. The boundaries of the immiscibility at these temperatures are consistent with those of Frantz et al. (1992). These two datasets provide important insights into the phase conditions of this system under high *T-P* conditions. Useful data were also reported by Joyce and Holloway (1993). They measured the activity of water in the ternary system using f_{H_2} and f_{O_2} buffers. Based on the measured equilibrium activity-composition relation, they drew tie lines at 850°C and 2000 bar.

There are ten ternary parameters (see Table 5) to be evaluated. If all the ternary interaction parameters are equal to 1.0, it implies that the ternary interactions are negligible, and the ternary properties can be predicted on the basis of the three binary systems. However, our test indicates that ternary interaction parameters are indispensable for the reliable prediction of either phase behavior or volumetric properties, no matter how the binary parameters are adjusted. It was found that all the δ_{ijkl}'s can be set equal to each other with little effect on fitting. This is also true for all the ϵ_{ijklm}'s. Therefore, only three ternary parameters as a function of temperature (7 coefficients in total) (see Table 5) need to be adjusted. We evaluated the three ternary parameters based on the 2547 data points (calibrated) of Gehrig (1980), Takenouchi and Kennedy (1965), and Frantz et al. (1992). These data fall into the *T-P* range below 700°C and 3000 bar. In order to test the extrapolation of the EOS, we reserve the data of Johnson (1991), Joyce and Holloway (1993), and Kotelnikov and Kotelnikova (1990), which cover *T-P* range up to 950°C and

Table 7. Prediction of Molar Volume (cc/mole) at High Temperatures and Pressures

T(C)	P(bar)	x(NaCl)	$x(H_2O)$	$x(CO_2)$	v(exp)*	v(EOS)**
938	7458	.0410	.7720	.1870	27.67	27.92
930	6600	.0352	.6848	.2800	30.78	30.81
924	6800	.0244	.4866	.4890	35.60	34.56
940	7400	.0617	.6483	.2900	29.96	29.94

* The experimental data are from Johnson (1992)

** calculated mole volume (cm^3/mole)by the EOS of this study.

Table 8. The Excess Volume* (cc/mole)

T(°C)	P(bar)	V_{mix}	V_{ex}
400	500	49.73	6.48
400	1000	34.89	1.35
400	2000	28.98	0.39
500	500	73.05	23.77
500	1000	41.79	4.65
500	2000	31.21	0.79
700	500	118.47	7.04
700	1000	60.84	9.52
700	2000	38.00	2.4
700	5000	27.53	-0.08

* $v'_{ex}=v_{mix}-0.2v_{CO2}-0.8v_{NaCl-H_2O}$ with $x_{NaCl}/x_{H2O}=0.25$

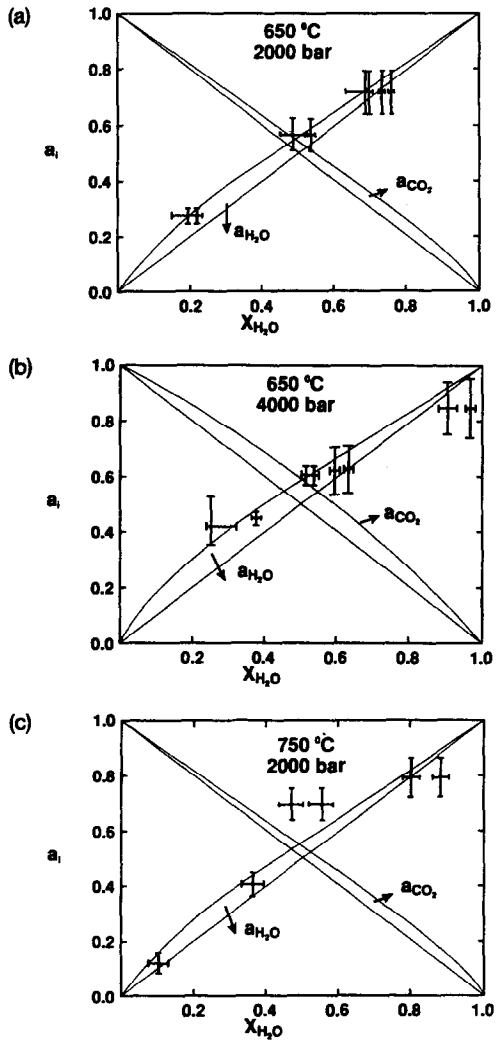

FIG. 9. (a)–(c) The activities of H_2O and CO_2 at high temperatures and pressures. The cross bars are the experimental measurements of Joyce and Holloway (1993). The curved solid lines are the calculation of this EOS. The diagonal solid lines represent ideal mixing.

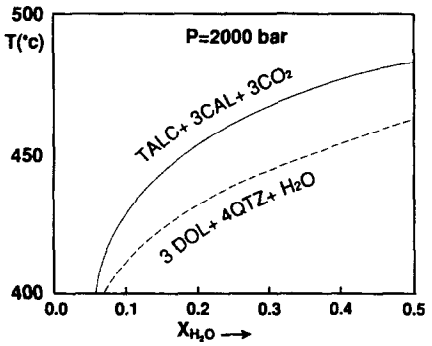

FIG. 10. The *P-T* boundaries for the reaction 3 dolomite + 2 quartz + H_2O = talc + 3 calcite + $3CO_2$ in the absence of NaCl (dashed line) and with the addition of 0.1 mole fraction of NaCl (solid line).

7500 bar. As shown below, the EOS is valid over a much broader *T-P* range than the range for the parameter evaluation.

4. COMPARISON WITH EXPERIMENTAL DATA

The reliability and accuracy of an EOS must be determined by comparison with experimental data. Here, we demonstrate the capability of this EOS to predict both phase equilibria (or immiscibilities) and volumetric properties (*PVTX*) in the ternary system.

Figure 2a,b compares the EOS calculation of the liquid-vapor equilibria with experimental data at 300 and 350°C, respectively. In this figure, the NaCl concentration is not shown on the vapor side because it is so small. The figure

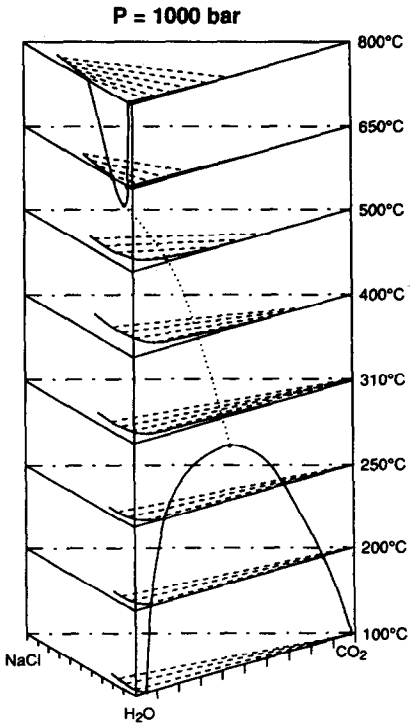

FIG. 11. The phase diagram of the system NaCl–H_2O–CO_2 at various temperatures and constant pressure of 1000 bar. The part below 300°C is calculated from the EOS of Duan et al. (1992b).

clearly demonstrates that the predictions of this EOS are within experimental accuracy under the conditions shown except near the critical range. It is interesting to note from these figures that the extent of immiscibility can be considerably increased over that of the CO_2-H_2O binary by the addition of NaCl.

The accuracy of this EOS in the prediction of phase equilibria (immiscibilities) is further shown by Figs. 3, 4, 5, 6, and 7. Figure 3 shows the close agreement of the prediction of phase coexistence measurements of Frantz et al. (1992). Figure 3a,b (see above) indicates that the immiscibility fields decrease with increasing pressure for a given temperature. The diagram at 800°C and 2000 bar of Kotelnikov and Kotelnikova (1990), given by Fig. 4, is well predicted by our EOS. Although we did not use any data above 700°C and 3000 bar in the parameterization, the immiscibility at 930°C and 7500 bar are well predicted as compared with the synthetic fluid inclusion measurement by Johnson (1991) (see Fig. 5). The data of Johnson (1991) are not sufficient to determine the tie lines. The tie lines between vapor-liquid phase equilibrium established by Joyce and Holloway (1993) are shown in Figs. 6 and 7. We show very good agreement with their data at 850°C and 2000 bar (Fig. 6). In Fig. 7, the tie line measured by Joyce and Holloway (1993) is in general agreement with our EOS. However, the schematic phase boundary they drew shows a substantially larger immiscibility field. Their data appear to be insufficient to draw this boundary.

Figure 8a–d displays the comparison of volumetric data with the EOS of this study for systems of various compositions. In these figures, the nearly straight lines are the predicted isochores, the dashed lines are predicted phase boundaries, and the solid dots are the experimental *PVT* data of Gehrig (1980). It can be seen that the EOS is very close to the experimental data (within an error of about 6–7% in volume) under various conditions. Table 6 indicates that the EOS of Bowers and Helgeson (1983a) has much larger errors. The errors in the low pressure range will lead to big errors in the evaluating fugacities or chemical potentials. Because NaCl is treated as ion-pair molecules in the EOS and it partially dissociates below 350°C, the accuracy decreases slightly below 350°C. Although the parameters in this EOS are evaluated from data below 700°C and 3000 bar, the volume measurements over 920°C and 7000 bar of Johnson (1992) are accurately predicted (see Table 7).

5. PREDICTION OF PROPERTIES

Excess volumes, activities, isochores, and phase equilibria can be determined from the EOS. All these properties are important in the understanding of fluid behavior under various geological conditions.

5.1. Excess Volume

The excess volume is defined as:

$$v_{ex} = v_{mix} - \sum_i^n x_i v_i . \quad (36)$$

We have previously discussed the excess volume in the $CH_4-CO_2-H_2O$ system (Duan et al., 1992b) and shown that it can be a large percentage of the total volume. In the $NaCl-H_2O$ system, the excess volume can be both very negative and positive. For example, at 400°C and 1000 bar, the excess volume of the system $0.1NaCl + 0.9H_2O$ is −47.9 cubic centimeter (cc) when the total volume is 23.1 cc. The accuracy of the ideal geometric mixing approach of Brown and Lamb (1989) can be assessed by calculating the excess volume defined as

$$v'_{ex} = v_{mix} - x_{CO_2} v_{CO_2} - (1 - x_{CO_2}) v_{NaCl-H_2O}, \quad (37)$$

where v_{mix} is the molar volume of the ternary mixed system and v_{NaCl-H_2O} is molar volume of the binary under the same *T-P* condition and same x_{NaCl}/x_{H_2O} ratio. It can be seen from Table 8 that the excess volume amounts to about 7–30% of the total volume for pressures below 2000 bar, and about 0–5% for pressures above 2000 bar. This implies that the approach (see above) of Brown and Lamb (1989) may give approximate result for pressures above 2000 bar, but incorrect results for pressures below 2000 bar.

5.2. Activities

The activity of a species i is defined as

$$a_i = x_i \phi_i / \phi_i^0 , \quad (38)$$

where ϕ_i^0 is the fugacity coefficient of species i in its pure state. The equations for calculating fugacity coefficients are listed in the Appendix. Comparison of the calculated activities in the binary H_2O-CO_2 with the data of Joyce and Holloway (1993), as shown in Fig. 9, indicates that our calculations are in good agreement with experimental data except at the water-rich end. The activity measurements in the ternary $NaCl-H_2O-CO_2$ by Joyce and Holloway (1993) enabled them to draw a tie line between liquid and vapor phase equilibrium. This tie line is well predicted by our EOS as shown in Figs. 6 and 7. Note that the data of J + H were not used in the evaluation of the parameters.

As stated before, adding NaCl in the H_2O-CO_2 system can dramatically change the activities of both H_2O and CO_2. For example, at 450°C and 2000 bar, the fugacity coefficients of H_2O and CO_2 in the system $0.6H_2O + 0.4CO_2$ are 0.316 and 2.404, respectively. However, adding 0.1 mole fraction of NaCl and keeping the H_2O to CO_2 ratio constant, these fugacity coefficients change to 0.222 and 4.607, respectively. This change in activity has a substantial effect on alteration reactions. For example, consider the decarbonation and dehydration reaction:

$$3CaMg(CO_3)_2(\text{dolomite}) + 4SiO_2(\text{quartz}) + H_2O = Mg_3Si_4O_{10}(OH)_2(\text{talc}) + 3CaCO_3(\text{calcite}) + 3CO_2 \quad (39)$$

in the system $CaO-MgO-SiO_2-H_2O-CO_2$ (Bowers and Helgeson, 1983b). Adding 0.1 mole fraction NaCl relative to $NaCl + H_2O + CO_2$, the stability field of the minerals will shift substantially as shown in Fig. 10.

5.3. Calculation of Isochores, Homogenization Temperatures, Pressures, and Immiscibilities

Using microthermometric technique together with Raman spectrometry analyses, it is possible to find out the total composition and total homogenization temperatures (Ramboz et al., 1985; Williams-Jones and Ferreira, 1989; Diamond, 1990). According to the composition analyzed, a constant composition diagram with phase relations and isochores can be calculated. This kind of diagram determines the homogenization pressures (internal pressure) for a given homogenization temperature. With the known temperature, pressure, and composition, the volume can be calculated. Isochores can be calculated as needed. Such calculations are illustrated by Fig. 8a–d. The curved dashed lines in these figures are phase boundaries. This boundary also represents homogenization *T-P* curve. Above this curve, the system is homogeneous. Below this curve, the fluid separates into liquid and vapor phase. The compositions of the liquid and vapor phase can be determined from the EOS. The end of these dashed lines should be close to critical region. The nearly straight lines are isochores.

The immiscibility can be better illustrated by a three dimension phase diagram. Such a diagram can be calculated from the EOS. Figure 11 is a constant pressure diagram showing the phase relations under varying temperatures. It can be seen that the immiscibility field is minimal around 400°C. Above or below this temperature the immiscibility field expands. The dashed line A-B connects the critical points of various temperatures. Above 640°C, there are no critical points. The dashed straight lines are tie-lines representing liquid-vapor coexistence. The tie lines indicate that very highly saline brines may result from phase separation under high temperatures. More details on the relationship between the immiscibility and mineralization will be discussed in a separate publication (Hu et al., 1995).

Acknowledgments—We thank Drs. A. Anderko, K. S. Pitzer, and John Wheeler for valuable discussions. This work has been supported by funds from the Department of Energy: DE-FG07-93ID13247, University Energy Research Group, Central Canada Potash, and Unocal Science and Technology Division. Drs. I.-M. Chou, M. Sterner, R. Bodnar, and M. McKibben are acknowledged for their constructive reviews.

Editorial handling: M. A. McKibben

REFERENCES

Alston R. B., Kokolis G. P., and James C. F. (1985) CO_2 minimum miscibility pressure: A correlation of impure CO_2 streams and live oil system. *Soc. Pet. J.* **25,** 268–274.

Anderko A. and Pitzer K. S. (1993) Equation of state representation of phase equilibria and volumetric properties of the system NaCl–H_2O above 573 K. *Geochim. Cosmochim. Acta* **57,** 1657–1680.

Bischoff J. L. (1980) Geothermal system at 21°N, East Pacific Rise: Physical limits on geothermal fluid and role of adiabatic expansion. *Science* **207,** 1465–1469.

Bodnar R. J. (1985) Pressure-volume-temperature-composition (*PVTX*) properties of the system H_2O–NaCl at elevated temperatures and pressures. Ph.D. dissertation, Penn. State Univ.

Boublik T. (1970) Hard sphere equation of state. *J. Chem. Phys.* **53,** 471–472.

Bowers T. S. and Helgeson H. C. (1983a) Calculation of the thermodynamic and geochemical consequences in the system H_2O–CO_2–NaCl on phase relations: Equation of state for H_2O–CO_2–NaCl fluids at high pressures and temperatures. *Geochim. Cosmochim. Acta* **47,** 1247–1275.

Bowers T. S. and Helgeson H. C. (1983b) Calculation of the thermodynamic and geochemical consequences in the system H_2O–CO_2–NaCl on phase relations: Metamorphic equilibria at high pressures and temperatures. *Amer. Mineral.* **68,** 1059–1075.

Brown P. E. and Lamb W. M. (1989) *P-V-T* properties of fluids in the system $H_2O \pm CO_2 \pm$ NaCl: New graphical presentations and implications for fluid inclusion studies. *Geochim. Cosmochim. Acta* **53,** 1209–1221.

Carnahan N. F. and Starling K. E. (1969) Equation of state for nonattracting rigid spheres. *J. Chem. Phys.* **51,** 635–636.

Crawford M. L. (1981) Phase equilibria in aqueous fluid inclusions. *Mineral. Assoc. Can. Short Course Handb.* **6,** 75–100.

Diamond L. W. (1990) Fluid inclusion evidence for *P-V-T-X* evolution of hydrothermal solutions in late alpine gold-quartz veins at Brusson, Val d'Ayas, Northwest Italian Alps. *Amer. J. Sci.* **290,** 912–958.

Dimitrelis D. and Prausnitz J. M. (1986) Comparison of two hard-sphere reference systems for perturbation theories for mixtures. *Fluid Phase Equilibria* **31,** 1–21.

Duan Z., Møller N., and Weare J. H. (1992a) An equation of state for the CH_4–CO_2–H_2O system: I. Pure systems from 0 to 1000°C and 0 to 8000 bar. *Geochim. Cosmochim. Acta* **56,** 2605–2617.

Duan Z., Møller N., and Weare J. H. (1992b) An equation of state for the CH_4–CO_2–H_2O system: II. mixtures from 50 to 1000°C and from 0 to 1000 bar. *Geochim. Cosmochim. Acta* **56,** 2619–2631.

Franck E. U. and Todheide K. (1959) Thermische Eigenschaften Uberkristischer Mischungen von Kohlendioxyd und Wasser bis zu 750°C and 2000 bar. *Z. Phys. Chem. Neue Folge* **22,** 232–245.

Frantz J. D., Popp R. K., and Hoering T. C. (1992) The compositional limits of fluid immiscibility in the system H_2O–NaCl–CO_2 as determined with the use of synthetic fluid inclusions in conjunction with mass spectrometry. *Chem. Geol.* **98,** 237–255.

Gehrig M. (1980) Phasengleichgewichte und *pVT*-Daten ternärer Mischungen aus Wasser, kohlendioxid und Natriumchlorid bis 3 kbar and 550°C. Doctorate dissertation, Univ. Karlsruhe.

Gjothiem K., Heggelund P., Krohn C., and Motznildi K. (1962) On the solubility of CO_2 on molten halides. *Indes. Acta Chem. Scand.* **16,** 689–694.

Gubbins K. E. and Twu C. H. (1978) Thermodynamics of polyatomic fluid mixtures—I. Theory. *Chem. Eng. Sci.* **33,** 863–878.

Hanor J. S. (1979) The sedimentary genesis of hydrothermal fluids. In *Geochemistry of Hydrothermal Ore Deposits* (ed. H. L. Barnes), pp. 137–168. Wiley-Interscience.

Johnson E. L. (1991) Experimentally determined limits for H_2O–CO_2–NaCl immiscibility in granulites. *Geology* **19,** 925–928.

Johnson E. L. (1992) An assessment of the accuracy of isochore location techniques for H_2O–CO_2–NaCl fluids at granulite facies pressure-temperature conditions. *Geochim. Cosmochim. Acta* **56,** 295–302.

Joyce D. B. and Holloway J. R. (1993) An experimental determination of the thermodynamic properties of H_2O–CO_2–NaCl fluids at high temperatures and pressures. *Geochim. Cosmochim. Acta* **57,** 733–746.

Kotelnikov A. R. and Kotelnikova Z. A. (1990) Experimental study of phase state of the system H_2O–CO_2–NaCl by method of synthetic fluid inclusions in quartz. *Geokhimiya* **N4,** 526–537.

Mansoori G. A., Carnahan N. F., Starling K. E., and Leland T. W. (1971) Equilibrium thermodynamic properties of the mixture of hard spheres. *J. Chem. Phys.* **54,** 1523–1525.

Mather A. E. and Franck E. U. (1992) Phase equilibria in the system carbon dioxide water at elevated pressures. *J. Phys. Chem.* **96,** 6–8.

Ramboz C. (1979) Fluid inclusion study of the copper mineralization in the Southwest Tintic District (Utah). *Bull. Soc. Fr. Mineral.* **102,** 622–632.

Ramboz C., Schnapper D., and Dubessy J. (1985) The *P-$\bar{V}$-T-X-f*O_2 evolution of H_2O–CO_2-CH_4-bearing fluid in a wolframite vein: Reconstruction from fluid inclusion studies. *Geochim. Cosmochim. Acta* **49,** 205–219.

Rushbrooke G. S., Stell G., and Høye J. S. (1973) Theory of polar fluids. I. Dipolar hard spheres. *J. Mol. Phys.* **26,** 1199–1215.

Shmulovich K. I., Shmonov V. M., Mazur V. A., and Kalinichev A. G. (1980) *P-V-T* and activity concentration relations in the H_2O–CO_2 system (homogeneous solutions). *Geochem. Intl.* **17,** 123–139.

Skryjek R. and Vera J. H. (1986) An improved Peng-Robinson equation of state for pure compounds and mixtures. *Canadian J. Chem. Eng.* **64,** 323–333.

Stell G., Rasaiah J. C., and Narang H. (1972) Thermodynamic perturbation theory for simple polar fluids I. *J. Mol. Phys.* **23,** 393–406.

Stell G., Rasaiah J. C., and Narang H. (1974) Thermodynamic perturbation theory for simple polar fluids, II. *J. Mol. Phys.* **27,** 1393–1414.

Sterner S. M. and Bodnar R. J. (1991) Synthetic Fluid Inclusions *X*: Experimental determination of *P-V-T-X* properties in the CO_2–H_2O system to 6 kb and 700°C. *Amer. J. Sci.* **291,** 1–54.

Takenouchi S. and Kennedy G. C. (1964) The binary system CO_2–H_2O at high temperature and pressures. *Amer. J. Sci.* **262,** 1055–1074.

Takenouchi S. and Kennedy G. C. (1965) The solubility of carbon dioxide in NaCl solutions at high temperatures and pressures. *Amer. J. Sci.* **263,** 445–454.

Todheide K. and Franck E. U. (1963) Das Zweiphasengebiet und die Kritische Kurve in System kohlendioxide-Wasser bis zu Drucken von 3500 bar. *Z. Phys. Chem. Neue Folge* **37,** 387–401.

Truesdell A. H. (1993) Gas and isotope geochemistry of Geysers steam. In *Geothermal Reservoir Technology Research Program: Abstracts of Selected Research Projects,* pp. 68–69.

Twu C. H., Gubbins K. E., and Cray C. G. (1975) Excess thermodynamic properties for liquid mixtures of non-spherical molecules. *J. Mol. Phys.* **29,** 713–729.

Welhan J. A. and Craig H. (1979) Methane and hydrogen in East Pacific Rise hydrothermal fluids. *Geophy. Res. Lett.* **6,** 829–831.

Williams-Jones A. E. and Ferreira D. R. (1989) Thermal metamorphism and H_2O–CO_2–NaCl immiscibility at Patapedia, Quebec: evidence from fluid inclusions. *Contrib. Mineral. Petrol.* **102,** 247–254.

Zakirov I. V. (1984) The *P-V-T* relations in the H_2O–CO_2 system at 300 and 400°C. *Geochem. Intl.* **21,** 13–20.

APPENDIX: CALCULATION OF FUGACITY COEFFICIENTS

A few errors in the equations of Anderko and Pitzer (1993) are corrected here. The fugacity coefficient ϕ_i is given by:

$$\ln \phi_i = \frac{\mu_i - \mu_i^{ig}}{RT} - \ln Z, \tag{A1}$$

where $(\mu_i - \mu_i^{ig})$ is the difference between the chemical potential of component i in the real system and that in the ideal gas state. It is given by the sum of the hard-sphere, dipolar, and perturbation contributions:

$$(\mu_i - \mu_i^{ig}) = \Delta\mu_{i,hd} + \Delta\mu_{i,dip} + \Delta\mu_{i,per}. \tag{A2}$$

The hard-sphere contribution is expressed as

$$\frac{\Delta\mu_{i,hd}}{RT} = \left(\frac{\partial\left(\frac{na_{hd}}{RT}\right)}{\partial n_i}\right)_{v,T,n_{j\neq i}} + Z - 1, \tag{A3}$$

where

$$\frac{a_{hd}}{RT} = \frac{\frac{3DE}{F}\eta - \frac{E^3}{F^2}}{1-\eta} + \frac{\frac{E^3}{F^2}}{(1-\eta)^2} + \left(\frac{E^3}{F^2} - 1\right)\ln(1-\eta), \tag{A4}$$

$$\left(\frac{\partial\left(\frac{na_{hd}}{RT}\right)}{\partial n_i}\right)_{v,T,n_{j\neq i}} = \frac{a_{hd}}{RT} + \left(\frac{\partial\left(\frac{a_{hd}}{RT}\right)}{\partial x_i}\right)_{v,T,x_{j\neq i}} - \sum_{j=1}^{m} x_j \left(\frac{\partial\left(\frac{a_{hd}}{RT}\right)}{\partial x_j}\right)_{v,T,x_{j\neq i}}, \tag{A5}$$

where

$$\left(\frac{\partial\left(\frac{a_{hd}}{RT}\right)}{\partial x_i}\right)_{v,T,x_{j\neq i}} = \frac{\partial\left(\frac{a_{hd}}{RT}\right)}{\partial D}\frac{\partial D}{\partial x_i} + \frac{\partial\left(\frac{a_{hd}}{RT}\right)}{\partial E}\frac{\partial E}{\partial x_i} + \frac{\partial\left(\frac{a_{hd}}{RT}\right)}{\partial F}\frac{\partial F}{\partial x_i}, \tag{A6}$$

where D, E, and F are given by Eqns. 6–9 and

$$\frac{\partial\left(\frac{a_{hd}}{RT}\right)}{\partial D} = \frac{\frac{3E\eta}{F}}{(1-\eta)}, \tag{A7}$$

$$\frac{\partial\left(\frac{a_{hd}}{RT}\right)}{\partial E} = \frac{\frac{3D\eta}{F} - \frac{3E^2}{F^2}}{(1-\eta)} + \frac{\frac{3E^2}{F^2}}{(1-\eta)^2} + \frac{3E^2}{F^2}\ln(1-\eta), \tag{A8}$$

and

$$\frac{\partial\left(\frac{a_{hd}}{RT}\right)}{\partial F} = \frac{\frac{\eta}{F} + \frac{E^3}{F^3}(2-\eta)}{(1-\eta)} + \frac{\frac{3DE}{F}\frac{\eta^2}{F} - \frac{E^3}{F^3}(2+\eta)}{(1-\eta)^2} + \frac{\frac{2E^3\eta}{F^3}}{(1-\eta)^3} - 2\frac{E^3}{F^3}\ln(1-\eta). \tag{A9}$$

$$\frac{\partial D}{\partial x_i} = \sigma_i, \tag{A10}$$

$$\frac{\partial E}{\partial x_i} = \sigma_i^2, \tag{A11}$$

$$\frac{\partial F}{\partial x_i} = \sigma_i^3. \tag{A12}$$

The dipolar contribution is given by

$$\frac{\Delta\mu_{i,dip}}{RT} = \frac{\left(1 - \frac{2A_3}{A_2}\right)\frac{\partial(nA_2)}{\partial n_i} + \frac{\partial(nA_3)}{\partial n_i}}{\left(1 - \frac{A_3}{A_2}\right)^2}. \tag{A13}$$

The derivatives of A_2 and A_3 with respect to the number of moles of component i are

$$\frac{\partial(nA_2)}{\partial n_i} = -\frac{4}{3}\sum_{i=1}^{n}\sum_{j=1}^{n}\frac{b_i b_j}{b_{ij}^2}x_i x_j \eta_{ij}\tilde{\mu}_i^2\tilde{\mu}_j^2\left(\frac{\partial I_2}{\partial n_i}\right) - \frac{8}{3}\sum_{j=1}^{n}\frac{b_i b_j}{b_{ij}^2}x_j\eta_{ij}\tilde{\mu}_i^2\tilde{\mu}_j^2 I_2(\eta) \tag{A14}$$

$$\frac{\partial(nA_3)}{\partial n_i} = \frac{10}{9}\sum_{i=1}^{n}\sum_{j=1}^{n}\sum_{k=1}^{n}\frac{b_i b_j b_k}{b_{ij}b_{jk}b_{ik}}x_i x_j x_k \tilde{\mu}_i^2\tilde{\mu}_j^2\tilde{\mu}_k^2\eta_{ijk}^2\left(n\frac{\partial I_3}{\partial n_i}\right) + \frac{30}{9}\sum_{j=1}^{n}\sum_{k=1}^{n}\frac{b_i b_j b_k}{b_{ij}b_{jk}b_{ik}}x_j x_k \tilde{\mu}_i^2\tilde{\mu}_j^2\tilde{\mu}_k^2\eta_{ijk}^2 I_3(\eta), \tag{A15}$$

where

$$n\frac{\partial I_2}{\partial n_i} = \left(\frac{\partial(n\eta)}{\partial n_i} - \eta\right)(c_1 + 2c_2\eta + 3c_3\eta^2), \quad \text{(A16)}$$

$$n\frac{\partial I_3}{\partial n_i} = \left(\frac{\partial(n\eta)}{\partial n_i} - \eta\right)[(c_1 + 2c_2\eta + 3c_3\eta^2) \times (1 + c_4\eta + c_5\eta^2 + c_6\eta^3) + (1 + c_1\eta + c_2\eta^2 + c_3\eta^3)(c_4 + 2c_5\eta + 3c_6\eta^2)], \quad \text{(A17)}$$

$$\frac{\partial(n\eta)}{\partial n_i} = \frac{\sum_{j=1}^{n} x_j b_{ij}}{2v}. \quad \text{(A18)}$$

where b_{ij} is defined by Eqn. 17.

The perturbation contribution to the chemical potential is

$$\Delta\mu_{i,\text{per}} = -\frac{1}{RT}\left[\frac{1}{v}\left(\frac{1}{n}\frac{\partial(n^2a)}{\partial n_i}\right) + \frac{1}{4v^2}\left(\frac{1}{n^2}\frac{\partial(n^3acb)}{\partial n_i}\right) + \frac{1}{16v^3} \times \left(\frac{1}{n^3}\frac{\partial(n^4adb^2)}{\partial n_i}\right) + \frac{1}{64v^4}\left(\frac{1}{n^4}\frac{\partial(n^5aeb^3)}{\partial n_i}\right)\right] \quad \text{(A19)}$$

$$\frac{1}{n}\frac{\partial(n^2a)}{\partial n_i} = 2\sum_{j=1}^{n} x_j a_{ij}, \quad \text{(A20)}$$

$$\frac{1}{n^2}\frac{\partial(n^3acb)}{\partial n_i} = 3\sum_{j=1}^{n}\sum_{k=1}^{n} x_j x_k (ac)_{ijk} b_{ijk}, \quad \text{(A21)}$$

$$\frac{1}{n^3}\frac{\partial(n^4adb^2)}{\partial n_i} = 4\sum_{j=1}^{n}\sum_{k=1}^{n}\sum_{l=1}^{n} x_j x_k x_l (ad)_{ijkl} b^2_{ijkl}, \quad \text{(A22)}$$

$$\frac{1}{n^4}\frac{\partial(n^5aeb^3)}{\partial n_i} = 5\sum_{j=1}^{n}\sum_{k=1}^{n}\sum_{l=1}^{n}\sum_{m=1}^{n} x_j x_k x_l x_m (ae)_{ijklm} b^3_{ijklm}. \quad \text{(A23)}$$